Inorganic Chemistry

Article

pubs.acs.org/IC

Revised Bi/M Layered Oxo-Sulfate (M = Co, Cu): A Structural and Magnetic Study

Minfeng Lü,[†,‡] Marie Colmont,[†] Houria Kabbour,[†] Silviu Colis,[§] and Olivier Mentré*[,†]

[†]Unité de Catalyse et de Chimie du Solide (UCCS USTL), Université Lille Nord de France, UMR 8181 CNRS, F-59655 Villeneuve d'Ascq, France

[‡]State Key Laboratory of Rare Earth Resource Utilization, Changchun Institute of Applied Chemistry, Chinese Academy of Sciences, Changchun 130022, P. R. China

[§]Institut de Physique et Chimie des Matériaux de Strasbourg (IPCMS), UMR 7504 CNRS and Université de Strasbourg (UDS-ECPM), 23 rue du Loess, BP 43, 67034 Strasbourg Cedex 2, France

Supporting Information

ABSTRACT: The combination of oxo-bismuthite slabs with counter oxo-anions main often leads to a series of layered Sillen-related compounds. For electroneutrality, it is convenient that the structure incorporates aliovalent cations such as Bi^{3+}/M^{2+} ions that could be confined either in the Bi/O slabs or in the interleave. In the case of SO_4^{2-} oxo-anions, only two compounds have been reported for M = Co, Cu, while interesting magnetic topologies emerge in absence of any prior characterization. Our reinvestigation of these systems using crystal growth in Bi_2O_3 flux led to the full structural characterization of $[Bi_2CoO_3](SO_4)$ (I) and $[Bi_{6.2367}Cu_{1.6O8}](SO_4)_3$ (II), which both exhibit pleated [Bi/M/O] slabs running in doubled cells comparatively to previous reports. (I) shows an interesting weak ferromagnetism (~0.2 μ_B/Co) below 17 K arising from Dzyaloshinskii–Moriya interactions in Co^{2+} zigzag chains, while (II) is essentially a paramagnet despite the presence of Cu_2O_6 dimers. Finally in the novel $[Bi_6O_6](CoO_2)(SO_4)_2$ (III), the Co^{2+} ions are ordered with sulfate in the interleaves, leading to a noncentrosymmetric crystal structure.

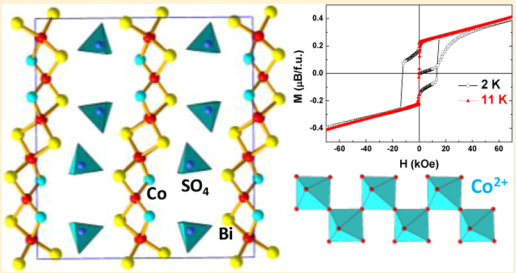

INTRODUCTION

The particular crystal chemistry of Bi^{3+} lone pair ions leads to unusual physical and chemical properties such as luminescence,[1] selective oxidation catalysts,[2,3] or multiferroic properties.[4] The combination between Bi_2O_3 and most voluminous anions (Cl^-, Br^-, I^-) or oxo-anions (IO^{3-},[5] SO_4^{2-},[6] CO_3^{2-}[7]) often leads to two-dimensional (2D) structural types related to the parent Sillen phases in which layered fluorite-like $[BiO]^+$ units host intercalated anions,[8,9] as shown in Figure 1a. These units are stabilized due to the ability of Bi^{3+} ions to form elementary oxo-centered tetrahedra OBi_4 or oxygen-deficient $O(Bi,\square)_4$ groups, where $\square$ defines vacancies. They most often share edges leading to various dimensionality of the framework, for example, three-dimensional (3D) in the highly condensed δ-Bi_2O_3 fluorite type (Figure 1b) against 2D in the $[BiO]^+$ slabs (Figure 1a). A review of all possible arrangements between OM_4 oxo-centered tetrahedra was recently published.[10] It highlights that in case of M = Bi^{3+}, the typical Bi^{3+}–O bond valence of 0.596 valence units (v.u.) (slightly higher than the 0.5 v.u. necessary to form ideal OBi_4 tetrahedra[11]) often results in the copresence of other M^{n+} cations into $O(Bi,M)_4$ units to relax the oxygen bonding scheme. In this context, our group has paid much attention to the case of phosphates with different M^{n+} cations and tuning M/Bi/PO_4 ratios. A variety of crystal structures has been obtained, for which a systematization was proposed in relation with the condensation between $O(Bi,M)_4$ tetrahedra.[12,13] Hence in the case of PO_4^{3-} oxo-anions, the incorporated M^{n+} ions can play the role of scissors that slice 2D $[BiO]^+$ units into versatile one-dimensional (1D) elementary ribbons, for instance, $[BiM^{2+}{}_2O_2]$ in $[BiM_2O_2](XO_4)$,[14,15] (see Figure 1c). But it could also preserve unchanged 2D $[BiO]^+$ distorted layers, while M^{n+} ions incorporate the anionic interleave, as seen in $[Bi_6O_6](TiO_2)(PO_4)_2$,[16,17] see Figure 1d. By analogy with the phosphate cases, we are strongly interested in the diversification of the anion source leading, for instance, to unexpected complex edifices such as the multi-dimensional combination of layers and channels in $Bi_{17}PbO_{22}Cl_9$.[18] For sulfate anions, to our knowledge, only a few terms have been reported. As far as we know, in addition to a handful of bismuth oxo-sulfates such as the 2D $Bi_{26}O_{27}(SO_4)_{12}$ built up of fluorite-like steps[19] only rare cases of mixed Bi/M oxo-sulfates are known. For instance, $[Bi_{1-x}Co_xO]_2(SO_4)_{1-x}$, where $0.14 \leq x \leq 0.18$,[20] adopts a Sillén-X1 phase.[8,9] More intriguing cases involve pleated oxo-centered layers found in both $[Bi_2CoO_3](SO_4)$[6] (Figure 1e) and $[Bi_{13.33}Cu_2O_{16}](SO_4)_6$[21] with segregation of the transition metals within the layers. However, in both cases, the examination of reported crystal structures highlights strong SO_4 disorder. Here we present a full reinvestigation of these

Received: April 16, 2014
Published: June 18, 2014

   dx.doi.org/10.1021/ic500877z | Inorg. Chem. 2014, 53, 6969–6978

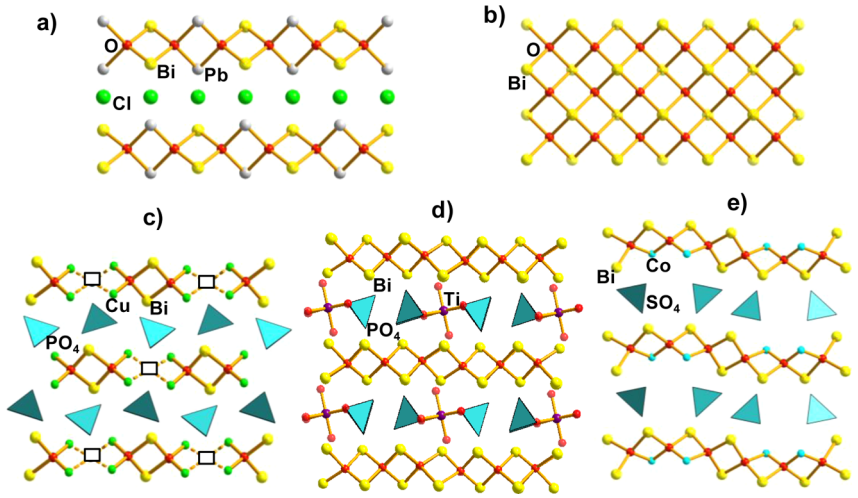

Figure 1. Various types of 1D, 2D, and 3D units with edge-sharing $O(Bi,M)_4$ tetrahedra: (a) 2D in $PbBiO_2Cl$, (b) 3D in δ-Bi_2O_3, (c) 1D in $[BiCu_2O_2](PO_4)$, (d) 2D in $[Bi_6O_6](TiO_2)(PO_4)_2$, and (e)2D in $Bi_2CoO_3(SO_4)$. Squares in $[BiCu_2O_2](PO_4)$ and dotted lines stand for missing atoms.

two latter compounds and their detailed magnetic properties. In addition, the crystal structure of the new $[Bi_6CoO_8](SO_4)_2$ compound is reported.

EXPERIMENTAL AND METHODS

Synthesis. *$[Bi_2CoO_3](SO_4)$ (I).* In the previous reports focused on the crystal structure of (I), single crystals were grown by heating a mixture of $Co(SO_4)\cdot 7H_2O$ and Bi_2O_3 in the ratio of Co/Bi = 3:2, see ref 6. In the present study, similar crystals were obtained by slow cooling during 100 h of a mixture of Bi_2O_3/CoO/$(NH_4)_2SO_4$ in the molar ratio of 1:2:2. The mixtures were first annealed at 723 K for 12 h after thoroughly grinding, and then they were put into a gold tube and vacuum-sealed in quartz tubes. Heat treatments were performed at 1173 K for 2.5 h and slowly dropped to 973 K at the rate of 2 K/h. Energy-dispersive X-ray (EDX) analyses of purple brick-shaped crystals indicate the presence of Bi, Co, and S as constituting elements in the ratio of Bi/Co/S = 2:0.8:1.2 in good agreement with the refined formula (Supporting Information, Figure S1). However, the determined unit cell is a = 5.4153(2), b = 14.2437(6), and c = 15.7595(7) Å, which corresponds to b doubling relatively to the original report.[6]

Among several attempts, the corresponding powder was obtained as a major polycrystalline component in a mixture from the stoichiometric mixture of Bi_2O_3 (Aldrich, 99.9%) and $CoSO_4\cdot 7H_2O$ (Carlo Erba, 99%). The reagents were weighted, placed in an agate mortar, closely ground and homogenized, deposited in a gold tube, and vacuum-sealed in quartz tubes. The treatment was performed at 1123 K for 2.5 h followed by a quick decrease to 993 K, followed by further cooling to 943 K in 200 h. The final product was nearly single phase (see Figure 2 and Table 1). The lattice parameters refined from the powder diffraction pattern led to a primitive orthorhombic structure with a = 5.4132(5), b = 14.227(1), and c = 15.753(1) Å, which is in good agreement with results from the single-crystal data (see Table 2).

$[Bi_{6.267}Cu_{1.6}O_8](SO_4)_3$ (II). Single crystals of II were originally prepared by heating in Pyrex-evacuated tubes a mixture of $Bi_2O(SO_4)$ and CuO in a Bi/Cu ratio = 2:1 (see ref 20). In our study, green bulk crystals were grown in the melt of a mixture of Bi_2O_3 + CuO + $(NH_4)_2SO_4$ (molar ratio = 1:1:2). After thoroughly grinding and mixing, the above-mentioned mixture was first heated at 723 K for 12 h, then loaded into gold tubes, and vacuum-sealed in silica tubes. Heat treatments were performed at 1253 K for 2.5 h, quickly cooled to 973 K, and finally cooled to 773 K (66.7 h). EDX analyses of isolated green bulky crystals showed the presence of copper as a constituting element but also showed, using a semiquantitative analysis (Supporting Information, Figure S2), the copresence of Bi/Cu/S with a ratio of 5:1.7:3, which is close to the results of our structural analyses. The refined unit cell parameters are a = 15.0204(9), b = 5.407(2), and c = 20.520(3) Å, which corresponds to a a axis doubling comparatively to the previous report.[21]

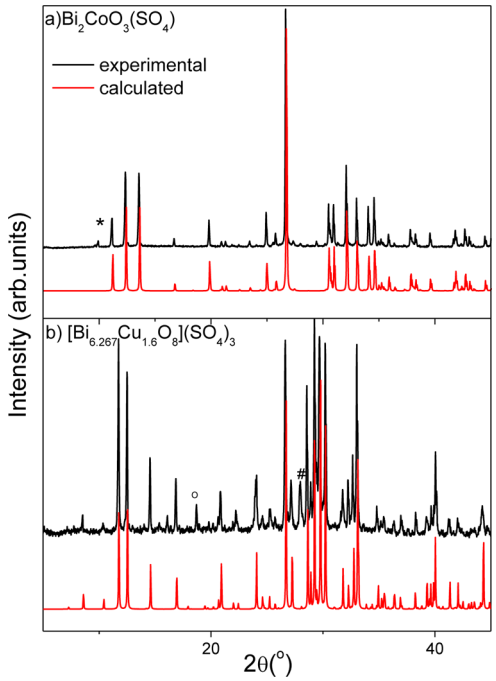

Figure 2. Experimental (black) and calculated (red) X-ray powder patterns for (a) $[Bi_2CoO_3](SO_4)$ and (b) $[Bi_{6.267}Cu_{1.6}O_8](SO_4)_3$. The marker * refers to phase with a slight chemical deviation, # indicates $Bi_{34.67}O_{36}(SO_4)_{16}$, and O indicates unknown impurities.

Several attempts were made to prepare single-phase polycrystalline (II), among which three experiments are detailed in Table 1. The most relevant result (i.e., compound (II) as a major component with minor additional phases) was obtained from the mixture of single-crystal products, as shown in Figure 2. The orthorhombic cell parameters refined from the powder diffraction are a = 15.0228(9), b = 5.4092(3), and c = 20.549(1) Å.

$[Bi_6O_6](CoO_2)(SO_4)_2$ (III). Pink transparent crystals were found in the melt of the mixture Bi_2O_3 + CoO + $(NH_4)_2SO_4$ (molar ratio = 1:2:1). The mixture was first heated at 773 K for 12 h after thoroughly

dx.doi.org/10.1021/ic500877z | Inorg. Chem. 2014, 53, 6969−6978

Table 1. Conditions and Results of the Attempts to Reproduce the Compounds in the Form of Powder

formulation	T, K	starting materials	conditions	identified phases[a]
$[Bi_2CoO_3](SO_4)$	973−1173	Bi_2O_3,$CoSO_4{\cdot}7H_2O$	evacuated tube	$Bi_2CoO_3SO_4$
	873	Bi_2O_3,$CoSO_4{\cdot}7H_2O$	evacuated tube	major, $Bi_2CoO_3SO_4$; minor, s.d.; minor, $Bi_{28}O_{32}(SO_4)_{10}$
	923	Bi_2O_3,$CoSO_4{\cdot}7H_2O$	evacuated tube	major, $Bi_2CoO_3SO_4$; minor, s.d.; minor, $Bi_{28}O_{32}(SO_4)_{10}$
$[Bi_{6.267}Cu_{1.6}O_8](SO_4)_3$	873	Bi_2O_3, CuO, $(NH_4)_2SO_4$	evacuated tube	$Bi_{34.67}O_{36}(SO_4)_{16}$; $CuBiO_4$; $Bi_2O(SO_4)_2$; u.p.
	943−1123	Bi_2O_3, CuO, $(NH_4)_2SO_4$	evacuated tube	major, $[Bi_{6.267}Cu_{1.6}O_8](SO_4)_3$; minor $Bi_{34.67}O_{36}(SO_4)_{16}$,
	923	Bi_2O_3,$CuSO_4{\cdot}5H_2O$	air	$Bi_{28}O_{32}(SO_4)_{10}$; u.p.

[a]Here, s.d. refers to slight chemical deviation from formulation, and u.p. denotes many unknown phases.

Table 2. Crystal Data, Measurement, and Structural Refinement Parameters of $[Bi_2CoO_3](SO_4)$, $[Bi_{6.267}Cu_{1.6}O_8](SO_4)_3$, and $[Bi_6O_6](CoO_2)(SO_4)_2$ with Comparison of Data from the Literature (References 6 and 21)

	$[Bi_2CoO_3](SO_4)$	$[Bi_2CoO_3](SO_4)$[6]	$[Bi_{6.267}Cu_{1.6}O_8](SO_4)_3$	$[Bi_{13.33}Cu_2O_{16}](SO_4)_6$[21]	$[Bi_6O_6](CoO_2)(SO_4)_2$
crystal data					
crys. symmetry space group	orthorhombic *Pbca*	orthorhombic *Pbcm*	orthorhombic *Pnma*	orthorhombic *Pmmn*	monoclinic *C*2
a (Å)	5.4153(2)	7.123(2)	15.0204(9)	20.550(3)	15.2834(14)
b (Å)	14.2437(6)	15.762(4)	5.407(2)	5.4364(11)	5.5468(5)
c (Å)	15.7595(7)	5.416(2)	20.520(3)	7.4851(11)	11.2272(10)
β (deg)					131.481(4)
V (Å^3)	1215.59(9)	608.07	1666.6(8)	836.2(3)	713.05(12)
Z	8	4	4	1	2
Dx (g/cm3)	6.7837	6.78	7.2812	7.44	7.603
μ (mm^{-1}) (for λ Kα = 0.7107 Å)	60.790	57.984	68.410	68.3	75.281
appearance	transparent, purple	dark, yellow	transparent, green	transparent, green	transparent, pink
data collection					
λ (Mo Kα) (Å)	0.710 73		0.710 73		0.710 73
scan mode	ω and φ		ω and φ		ω and φ
$\theta_{(min-max)}$ (deg)	2.58−33.07		1.68−33.17		2.42−33.18
R(int) (%)	3.64		4.4		4.56
recording reciprocal space	$-8 \le h \le 8$		$-22 \le h \le 22$		$-23 \le h \le 22$
	$-21 \le k \le 21$		$-8 \le k \le 8$		$-7 \le k \le 8$
	$-23 \le l \le 24$		$-31 \le l \le 31$		$-17 \le h \le 17$
refinement					
measured, independent, collected refl.	2310, 2085, 30 725		3461, 2883, 43 558		2616, 2312, 9457
no. of refined parameters	100		119		73
refin. method	F		F		F
$R1(F^2)$(obs)/$R1(F^2)$(all)	0.0220/0.0256		0.0407/0.0513		0.038/0.046
$wR2(F^2)$(obs)/$wR2(F^2)$(all)	0.0264/0.0268		0.0398/0.0472		0.0364/0.0374
$\Delta\rho_{max}$/ $\Delta\rho_{min}$ (e Å^{-3})	1.24/ −5.76		6.60/ −7.69		4.40/ −2.59

grinding and mixing. Then the above-mentioned mixture was loaded into gold tubes and vacuum-sealed in silica tubes. Heat treatments were performed at 1123 K for 2 h, and then the tubes were quickly cooled to 993 K and finally cooled to 943 K at the rate of 1 K/h. EDX analyses indicated the presence of Bi, Co, and S as constituting elements with a ratio of 6:0.8:1.7, in agreement with the expected one (Supporting Information, Figure S3).

X-ray Diffraction. The single-crystal X-ray diffraction (XRD) data of all the investigated samples were collected using a Bruker Apex Duo diffractometer with a Mo IμS microfocus tube (λ = 0.710 73 Å). The intensity data were extracted from the collected frames using the program SAINT-Plus 6.02.[22] Lattice parameters were defined from the complete data set. Absorption corrections were performed by multiscan method using SADABS.[23] Data collection and pertinent data of the refinements for three single crystals studied in this work are gathered in Table 2. Crystal data for compounds I, II, and III were deposited at CrysDATA@fiz-karlsruhe.de and were assigned to numbers 427594, 427593, and 427595, respectively. The analysis of polycrystalline samples was performed at room temperature in the 5−80° angular 2θ range (scan step width = 0.02°) using a D8 Advance Bruker AXS diffractometer, Cu Kα source).

Elemental Analysis. EDX analysis of single crystals was performed on a HITACHI S4700 Scanning Electron Microscope (SEM) operating at 20 kV and a current of 15 μA at different magnifications. Compositions were determined using a semiquantitative routine method.

Magnetic Measurements. Data for compounds I and II were measured on a MPMS SQUID-VSM (Quantum Design) magnetometer. Typical measurements were performed using zero field cooling (ZFC) and field cooling (FC) procedures under 0.02 and 0.1 T fields. Magnetization versus field [$M(H)$] variations were measured between 7 and −7 T at different temperatures. For compound III, only small single crystals in mixture were produced, which hampers the magnetic characterization.

DFT Calculations. Density functional theory (DFT) calculations were performed using the program VASP (Vienna ab initio simulation package).[24] The calculations were carried out within the generalized gradient approximation (GGA) for the electron exchange and correlation corrections using the Perdew−Wang[25] functional and the frozen core projected wave vector method.[26] Total energies calculations were carried out using GGA plus on-site repulsion (GGA+U)[27] method to account for the strong electron correlation associated with the 3d electrons on the Co ions. The energy cutoff for the plane waves was set to 400 eV, and the total energy convergence threshold was set to 10^{-6}. 52 k-points in the irreducible Brillouin zone were used for the calculations. To access the J values of compound (I),

dx.doi.org/10.1021/ic500877z | Inorg. Chem. 2014, 53, 6969−6978

the total energies of three ordered spin states, namely, ferromagnetic (FM) E_1 and the antiferromagnetic (AFM) E_2 and E_3 represented in Supporting Information, Figure S4 were calculated using GGA+U method in a supercell ($2a$, b, c). Accurate total energies could be obtained and were used to extract the J values. The energies of the ordered spin states are expressed using the spin Hamiltonian

$$\hat{H} = -\sum_{i<j} J_{ij}\hat{S}_i \cdot \hat{S}_j$$

where J_{ij} corresponds to the superexchange (SE) or super-super-exchange (SSE) parameters between the spin sites i and j. For compound (I), the equations related to each chosen configuration are reported in Supporting Information, Figure S4 underneath each corresponding spin repartition (equations E_1, E_2, E_3). N represents the number of unpaired spins per spin site (N = 3 for Co^{2+} high spin).

RESULTS AND DISCUSSION

$[Bi_2CoO_3](SO_4)$ (I). Evidence for the a, $2b$, c supercell compared to the model reported in ref 6 was given by the close inspection of precession frames calculated from the full data set (see the $hk0$ layer in Figure 3a). Its crystal structure was solved in the space group *Pbca*. The refinement was carried out by full-matrix least-squares minimization using F values with all the atoms treated with anisotropic thermal parameters. It yields $R1$ (all 2310 refl.) = 2.56%, $R1$ (2085 obs. refl. with $I > 2\sigma(I)$) = 2.20%. Thermal parameters of all oxygen atoms are quite reasonable in our model, while previous reports lead to abnormal values for sulfate oxygen corners owing to a certain disorder considered in the subcell. The refined positional and thermal parameters are given in Supporting Information, Tables S1 and S2, while selected bond distances and angles are listed in Supporting Information, Table S3.

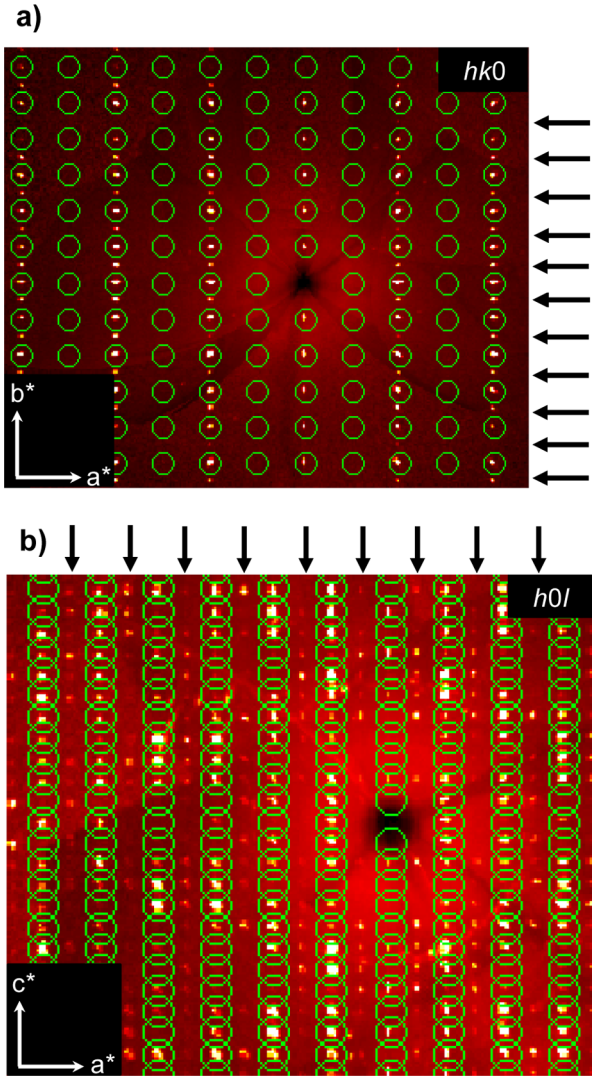

Figure 3. Calculated precession frame: (a) $hk0$ layer for compound (I) and (b) $h0l$ for compound (II). The arrows show supercell spots compared to refs 6 and 21 (indexed with green circles).

A projection of the structure of (I) in the *bc* plane is drawn in Figure 4a. Taking into account $O(Bi,Co)_4$ as the building units, $[Bi_2CoO_3](SO_4)$ consists of a 2D structure formed from the stacking of $_\infty[Bi_2CoO_3]$ sheet laying in the *ac* plane, isolated by $(SO_4)^{2-}$ tetrahedral groups. The a, $2b$, c supercell is mainly due to different tilting of SO_4 groups in the x, y, z and x, $y + 1/2$, z positions. The Co^{2+} ions are segregated on parallel rows perpendicular to the planes.

If one focuses on the coordination of the cations, it is remarkable that Bi and Co sites show a different coordination due to local distortion; that is, Bi(1) are surrounded by five O atoms, Bi(2) by eight O atoms, while Co form CoO_5 square pyramids, rather than the previously announced hexacoordination. Note that the pentacoordination of Co involves an average Co−O distance of 2.07 Å. The calculated bond valence sums (BVS) calculations using Bi−O (parameters from ref 28) and Co−O lead to 2.87, 3.07, and 1.83, respectively, for Bi(1), Bi(2), and Co sites, see Table 3.

The CoO_5 pyramids are arranged by corner sharing into $_\infty[Co^{2+}O_5]^{8-}$ zigzag chains running along the a axis. They are separated by 7.13 and 7.90 Å along the b and c axes, respectively (Figure 4a). The shared corners correspond to the O(3) ions involved in the O_4 equatorial planes with the O(1) ions. The O(6) atoms constitute the apex of the distorted square pyramid and also belong to the sulfate groups (see Figure 4b).

The zero field cooled and field cooled (ZFC−FC) temperature-dependent magnetizations were measured in the range of 2−300 K in an applied field of 200 and 1000 Oe for $[Bi_2CoO_3](SO_4)$ (Figure 5a). Below 23 K an abrupt increase of $M(T)$ concomitantly with a ZFC−FC divergence on further cooling signals the appearance of a ferromagnetic component. It is striking that below ∼10 K the moment value is independent of the temperature and of the applied field. The magnetization upon cooling under applied field of 200 Oe is about 1100 emu/mol. In the paramagnetic regime the magnetic susceptibility was approximated to M/H and could be fitted by a Curie−Weiss law $\chi = C/(T - \theta_{CW})$ leading to similar results for both 200 and 1000 Oe applied fields: $\theta_{CW} = -196.5$ K, $\mu_{eff} = 5.85\ \mu_B/Co^{2+}$. This μ_{eff} is significantly larger than the spin-only value (3.87 μ_B) expected for high-spin (HS) Co^{2+} (S = 3/2, $t_{2g}^5e_g^2$) ions. Indeed, an important orbital contribution is expected for magnetically anisotropic Co^{2+} ions. Despite the net moment evidenced at low temperature, the negative θ_{CW} value indicates significant dominating AFM interactions. Using the mean-field (MF) expression for the Curie−Weiss temperature, $\theta_{CW} = zJS(S + 1)/3k_B$, where z is the number of Co neighbors along the chains (z = 2), leads to $J_{MF}/k_B \approx -36.4$ K for S = 3/2.

The $M(H)$ magnetization curves recorded at 30, 15, 11, and 2 K are plotted in Figure 5b. At 30 K, $M(H)$ is typical of a paramagnet, while a soft weak FM behavior that appears below 23 K is signalled by an $M(T)$ abrupt increase. This weak FM is

dx.doi.org/10.1021/ic500877z | Inorg. Chem. 2014, 53, 6969−6978

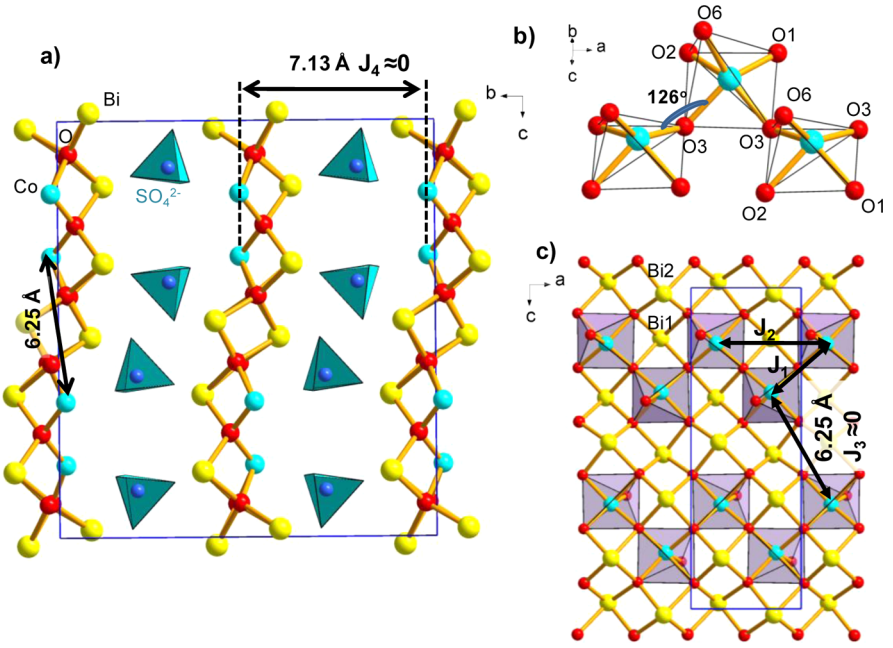

Figure 4. (a) Projection of the structure of $[Bi_2CoO_3](SO_4)$ (compound I) along the *a* axis with Bi, Co and O labels. (b) Geometry of the CoO_5 square pyramid coordination. (c) Projection of zigzag chains of CoO_5 square-pyramid along the *b* axis.

Table 3. BVS of the Three Examined Compounds

$[Bi_2CoO_3](SO_4)$ (I)				$[Bi_{6.267}Cu_{1.6}O_8](SO_4)_3$ (II)				$[Bi_6O_6](CoO_2)(SO_4)_2$ (III)			
atom	v_{Bi}[a]	V_{Co}[a]	V_S[a]	atom	v_{Bi}[a]	V_{Cu}[a]	V_S[a]	atom	v_{Bi}[a]	V_{Co}[a]	V_S[a]
Bi1	2.87			Bi1	2.52(3)			Bi1	2.84		
Bi2	3.07			Bi2	2.99(3)			Bi2	3.04		
Co		1.83		Bi3	2.97(3)			Bi3	3.01		
S			6.00	Bi4	2.88(3)			Co		1.98	
				Bi5	2.80(3)			S			6.12
				Bi6	2.75(3)						
				Bi7	4.81(12)						
				Cu7		1.39(4)					
				Cu		1.93(2)					
				S1			6.25(14)				
				S2 S3			6.15(19)5.96				

[a](R, b) parameters for Bi^{3+}–O (2.094, 0.37), Co^{2+}–O (1.692, 0.37), Cu^{2+}–O (1.679, 0.37), S^{6+}–O (1.624,0.37) are from ref 28.

characterized by a very weak coercive field. The related easy reversal of spins by inversing the applied field is reminiscent of low-dimensional magnetic units as evidenced in the 1D-FM Ising chains of $BaCo_2(As_3O_6)2)\cdot H_2O$,[29] 2D-FM Ising $BaFe^{2+}{}_2(PO_4)_2$,[30] or $Cs_2Ag^+F_4$.[31] At this stage of our study, it is most likely that the weak ferromagnetism is held by independent chains as discussed below. Finally in the $M(T)$ plateau below 10 K, the magnetization shows a hysteresis. Here, the 2D behavior turns into a 3D one due to interchain interactions that could be mediated by dipolar couplings as soon as the chain possesses a net magnetic moment. The observed steplike anomalies below 10 K are reminiscent of spring-exchange magnets. However, in such systems the interaction between soft and harder FM units is driving but should be excluded in compound (I). It is most likely related to grain reorientation upon field reversal as observed in $SrFe_3(PO_4)_3$, for which a strong dependence of the synthesis method on magnetization steps was evidenced.[32] The magnetization reached 0.4 μ_B/Co in an applied field of 7 T (Figure 5b), while the absence of saturation, that is, the steady increase of magnetization to 7 T, agrees with the dominating AFM behavior.

Four reasonable exchanges J_{1-4} were considered, according to geometrical considerations listed in Table 4. These interactions are shown in Figure 4c, while both interchain J_3 (diagonal between two chains) and J_4 (between two chains along *b*) can be assumed to be very weak. In the case of J_3, this is due to a Co–Co separation of 6.25 Å and a Co–O–O–Co torsion angle of 180°, which avoid magnetic contact by O 2p–O 2p σ overlap. For J_4 the superexchange path involves two long Co–O distances of 3.1 and 3.5 Å together with a Co–Co distance of 7.13 Å. The J values were calculated using the GGA +U approximation following the procedure detailed in the Experimental and Methods section. J_1–J_2 and the geometric characteristics related to each J are summarized in Table 4. The calculated J parameters are given in Table 5 for U_{eff} = 4 to 5 eV, consistent with the literature data for cobalt ions.[33] The obtained J values agree with empirically determined parameters using experimental magnetic measurements as detailed below. J_1 is found predominant (about 6 times larger) with respect to

dx.doi.org/10.1021/ic500877z | Inorg. Chem. 2014, 53, 6969–6978

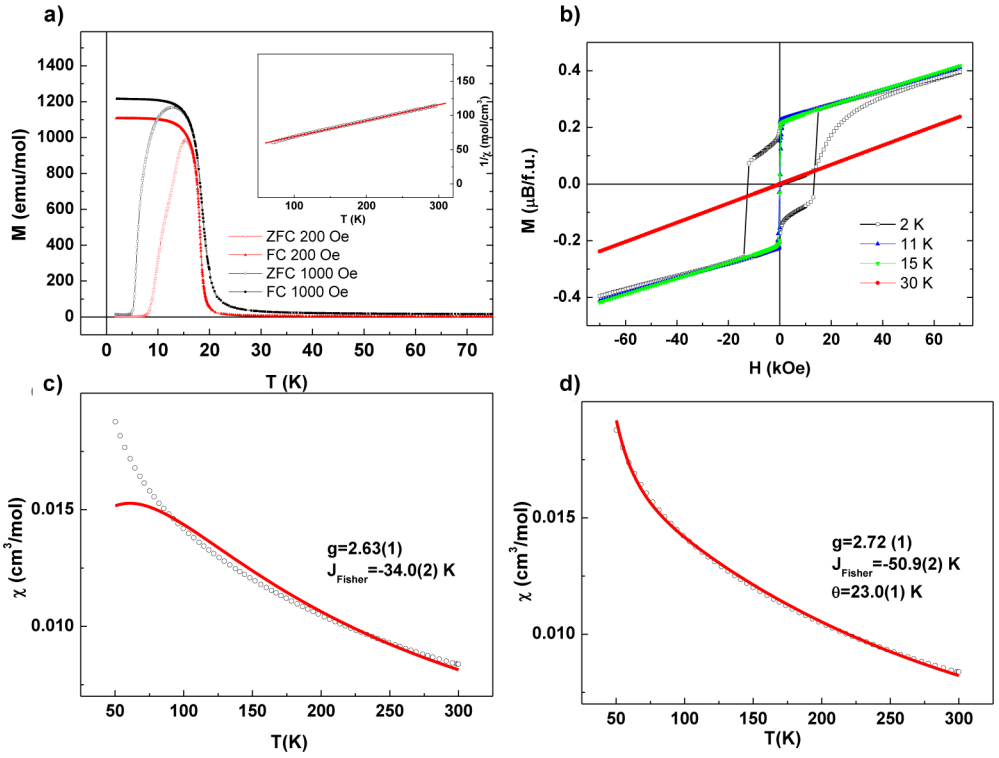

Figure 5. $[Bi_2CoO_3](SO_4)$ magnetic measurements. (a) Temperature dependence of the $[Bi_2CoO_3](SO_4)$ magnetic susceptibility: ZFC−FC plots under an external magnetic field of 200 and 1000 Oe. (inset) $1/\chi$ vs T, solid line corresponds to Curie−Weiss fit between 75 and 300 K. (b) Magnetization isotherm at 2, 11, 15 and 30 K. (c, d) χ vs T, solid line corresponds to the best fit for a Fisher 1D Heisenberg chain model and Weiss-term modified model.

Table 4. Description of Exchange Paths in $[Bi_2CoO_3](SO_4)$

J exchange type	path	M−M distances (Å)	M−X distances (Å)	angles (deg)
$J1$ (SE)	Co−O3−Co	3.61	Co−O3 = 2.03 O3−Co = 2.02	Co−O3−Co3 = 126
$J2$ (SSE)	Co−O3−O3−Co	5.41	Co−O3 = 2.03 O3−Co = 2.02 O3−O3 = 2.71	$_{Torsion}$Co−O3−O3−Co = 1.36
$J3$ (SSE)	Co−O1−O1−Co	6.25	Co−O1 = 2.07 O1−Co = 2.07 O1−O1 = 2.67	$_{Torsion}$Co−O1−O1−Co = 180
$J4$ (SSE)	Co−O6−O4−Co	7.13	Co−O6 = 2.06 O4−Co = 3.09 O6−O4 = 2.42	$_{Torsion}$Co−O6−O4−Co = 136

Table 5. Relative Energies of the Different Magnetic Configurations Used to Extract the Magnetic Exchange Parameters for Different U_{eff} Values

configuration[a]	relative E (eV)	J_1 (K)	J_2 (K)
U = 4 eV			
$E_{1\ (ferro)}$	0.4014	−64.70	−10.22
$E_{2\ (AF)}$	0		
$E_{3\ (AF)}$	0.1373		
U = 5 eV			
$E_{1\ (ferro)}$	0.3083	−49.69	−7.29
$E_{2\ (AF)}$	0		
$E_{3\ (AF)}$	0.1089		

[a]The most stable configuration is set to 0. The calculated J_{1-2} values are also given.

the weaker J_2 AFM coupling. It refutes the role of frustration inside the chains within J_1−J_2−J_2 triangles. Moreover, on the basis of the empirical criterion of the presence of frustration for $|\theta_{CW}|/T_c > 10$,[34] we find for $[Bi_2CoO_3](SO_4)$ a value of 9.2 out of the typical frustrated range. In absence of significant frustration possibly responsible for canting spins, the low-temperature magnetization is questionable. Indeed, in the context of important orbital moment contribution and asymmetric Co−O−Co J_1 exchanges (see Table 5), Dzyaloshinskii−Moriya interactions are most probably responsible for the weak ferromagnetism.

A fourth magnetic configuration (E_4) (see Supporting Information, Figure S4) was also investigated within our DFT calculations to evaluate possible interactions between the chains via J_3 in the *ac* plane, by comparison to the ferromagnetic configuration E_1. All *in-chain* spins interactions are set FM, while all *interchains* spin interactions are set AFM. It results in a

dx.doi.org/10.1021/ic500877z | Inorg. Chem. 2014, 53, 6969−6978

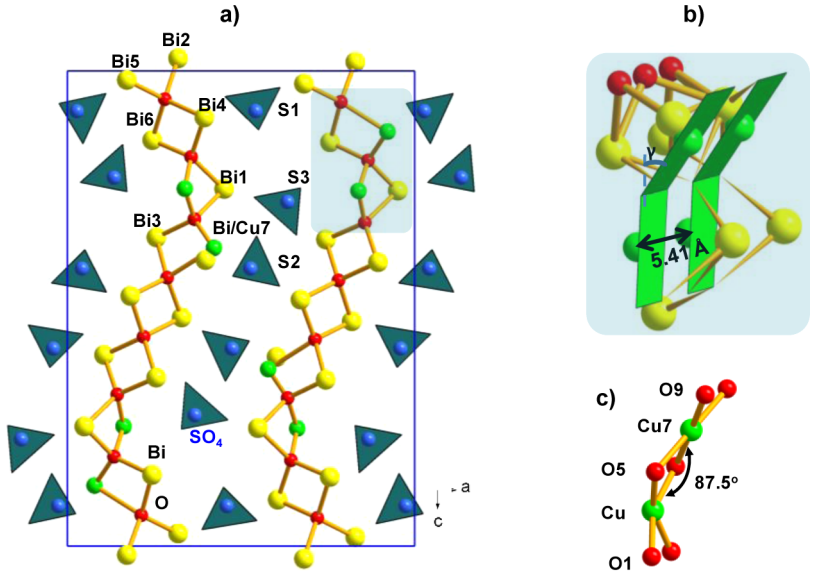

Figure 6. (a) The crystal structure of $[Bi_{6.267}Cu_{1.6}O_8](SO_4)_3$ (compound II). (b) Local structure of isolated dimers, edge-connected CuO_4 square planars are highlighted in green. (c) Geometry of the CuO_4 square planar coordination.

very small $|E_1 - E_4|$ difference = 0.0017 eV (at U_{eff} = 5 eV), which supports negligible magnetic exchanges between chains.

Following these results and main chainlike topology, the product $\chi T(T)$ at 1000 Oe above 50 K was fitted using a Fisher 1D Heisenberg chain model[35] ($S = 3/2$, $\hat{H} = -J \sum_{j>i=1}^{n} \vec{S}_i \cdot \vec{S}_j$) as a rough approximation of the chains of anisotropic Co^{2+} ions concerned here. It leads to $J_{fisher}/k_B = -34.0(2)$ K and g = 2.63(1) (R^2 = 0.986 35), which are very similar to previous results from the MF approximation (Figure 5c). We note that the fit could be further improved adding a θ Weiss corrective term: equation $\chi = (Ng^2\beta^2 S(S+1))(1+u)/(3k(T-\theta))(1-u)$, where $u = \coth[JS(S+1)/kT] - [kT/JS(S+1)]$.

It leads to $J_{fisher}/k_B = -50.9(2)$ K, g = 2.72(1), and θ = 23.0(1) K (R^2 = 0.998) (see Figure 5d), which are in good agreement with our DFT calculations for U_{eff} = 5 eV (Table 5), thus comfirming the nonfrozen orbital contribution. The positive value of θ may take into account extra intrachain coupling but also the interactions between them, significant since a hysteresis is opened below $T \approx 12$ K.

$[Bi_{6.267}Cu_{1.6}O_8](SO_4)_3$ (II). The crystal structure of compound (II) was solved in the space group *Pnma* (refined parameters a = 15.0204(9), b = 5.407(2), and c = 20.520(3) Å). The doubled a cell parameter, comparative to that announced with the $[Bi_{13.33}Cu_2O_{16}](SO_4)_6$,[21] was confirmed by calculated precession frame of the h0l layer from single-crystal XRD data (Figure 2b). A unit weighting scheme improves the convergence, with consideration of weaker supercell spots in this compound. Most of the structure is fully ordered, but the electron density on the Bi/Cu(7) position suggests a mixed occupancy with ratio of 0.38 for Bi and of 0.62 for Cu, respectively, as refined in split, is consistent with the observation on Fourier-difference maps. The presence of two different metals Bi/Cu(7) was validated by the BVS shown in Table 3. The predominant Cu^{2+} characterizes its mixed valence due to under bonding, while the complementary Bi (40%) seems over-bonded. For the simplicity, it was finally fixed to 0.4/0.6. Concomitantly, to balance the total charge, the occupancy of Bi atom of different sites was checked. A clue of lower than 100% occupancy on the basis of reasonable thermal parameters suggests a small degree of disorder within Bi(2)−Bi(5) sites, as shown in Supporting Information, Table 4S. The occupancies were then refined under restrictions for the conservation of the electric neutrality, leading to the formula $[Bi_{6.267}Cu_{1.6}O_8](SO_4)_3$. The final refinement cycles led to $R1$ = 0.0407 and $wR2$ = 0.0398. Anisotropic displacement parameters and selected interatomic distances are given in Supporting Information, Tables S5 and S6, respectively. Note that Bi vacancies in similar fluorite-like layers were reported for $Bi_{4-x}V_2O_{11-\delta}$ phases.[36] In the previously announced structure, several sites associated with abnormally high thermal parameters denote disorder in the *a*, *b*, *c* subcell, in the *Pmmn* space group.

After consideration of the supercell spots, an almost fully ordered model was refined as shown in Figure 6a. As for compound II, it is formed of a folded fluorite-like $[(Bi,Cu)_2O_2]^{2+}$ layer parallel to the *bc* plane and is also formed of $O(Bi,Cu)_4$ units, interleaved with SO_4^{2-} groups. The Bi/Cu disorder over the M(7) site was revealed by high residual electronic density (ρ = 21.24 e^- $Å^{-3}$) before the site was considered as a mixed one. The Bi/Cu disorder is responsible for rather high thermal parameters on the neighboring $S(2)O_4$ group due to local influence of either Bo or Cu on the orientation of this oxo-anion. The segregation of Cu^{2+} sites in the layers is different from those of compound (I), leading to 60% of isolated Cu_2O_6 dimers formed by two nearly coplanar edge-connected CuO_4 square planars (Cu and Cu7 sites). The Cu atoms form CuO_4 groups with Cu−O distance of 1.95 Å, while Bi/Cu(7) atoms are surrounded by four oxygen atoms with loose (2.04−2.09 Å) Cu−O bond of average distance of 2.07 Å (Figure 6b,c). However, the distance of Cu(7)−O(9) (2.09 Å) is uncertain due to overlarge thermal parameters of O(9) atoms. We note that this inaccuracy on the next $S(2)O_4$ position led to BVS far from the expected values, that is, 4.81 and 1.39 for Bi and Cu, respectively. On the opposite, Bi(1)−Bi(6), S(1)−S(3) are found to be compatible for both cationic types by BVS calculations as listed in Table 3. These results support the above slightly disordered model. The pertinent distances are given in Supporting Information, Tables S6.

The magnetic units in compound II involve 40% of isolated CuO_4 planes and 60% of $[Cu_2O_6]^{8-}$ dimers. In the latter, the

dx.doi.org/10.1021/ic500877z | Inorg. Chem. 2014, 53, 6969−6978

Cu−Cu distance is 2.85 Å, expected to be associated with weakly AFM exchanges since the Cu−O−Cu angle (87.5°) is very close to orthogonality.[37] An important deviation from planarity (hinge angle γ = 31°,) leads to roof-shaped Cu_2O_6 dimers. As a matter of fact similar topology inside dimers for $[BiCu_2O_2](PO_4)$ was associated with minor couplings compared to predominant ones between the dimers.[38] In addition, the hinge distortion between CuO_4 planes was established to reduce the antiferromagnetic coupling.[39]Along the *b* axis, between the dimers the minimal Cu−Cu separation is found close to 5.4 Å, which together with the Bi/Cu disorder is also expected to break long-range exchanges.

The magnetic data for compound II are shown in Figure 7a,b in the form of χ and $1/\chi$ plotted as a function of the temperature. The magnetization was corrected from diamagnetism, which is a necessary step in such dilute magnetic samples. Temperature dependence of magnetic data show Curie−Weiss behavior, $\chi = C/(T - \theta_{CW})$, with a Weiss constant (θ_{CW} = −0.2 K), suggesting very weak AFM interactions between Cu^{2+} ions in a dominating paramagnetic context. Furthermore, the effective moment estimated from Curie−Weiss fit is 1.69(2) μ_B/Cu, which is close to the spin-only value of 1.73 μ_B/Cu for S = 1/2 ions. No discrepancy was observed between the FC and ZFC curves (Figure 7a). This paramagnetic behavior was confirmed by fitting $M(H)$ the magnetization versus field at 2 K using a Brillouin function for isolated spins; we find g = 1.92(2) and S = 0.40(1), which approaches expected values (R^2 = 0.999), see Figure 7c.

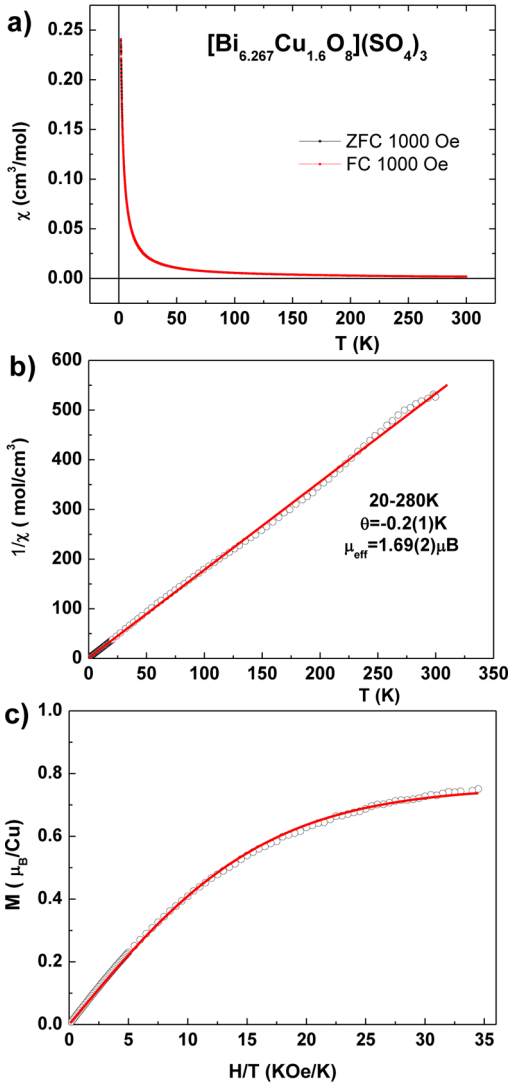

Figure 7. $[Bi_{6.267}Cu_{1.6}O_8](SO_4)_3$ magnetic measurements. (a) Temperature dependence of the $[Bi_{6.267}Cu_{1.6}O_8](SO_4)_3$ magnetic susceptibility: reversible ZFC−FC plots under an external magnetic field of 1000 Oe. (b) $1/\chi$ vs T, solid line corresponds to Curie−Weiss fit between 20 to 280 K. (c) M vs H/T, solid line corresponds to the best fit to the calculated Brillouin function for paramagnetic state.

$[Bi_6O_6](CoO_2)(SO_4)_2$ (III). The crystal structure of compound (III) was solved in the space group $C2$ with unit cell parameters of a = 15.2834(14) Å, b = 5.5468(5) Å, c = 11.2272(10) Å, and β = 131.48(2)°. The refinement was carried out by full-matrix least-squares minimization using F values with Bi, Co, and S atoms treated with anisotropic thermal parameters yielding $R1$ = 4.60% and $wR2$ = 3.74% (all 2616 reflections). The final refined formula is $[Bi_6O_6](CoO_2)(SO_4)_2$, considering the various engaged subunits shown in Figure 8a. We checked that the Bi positions are significantly

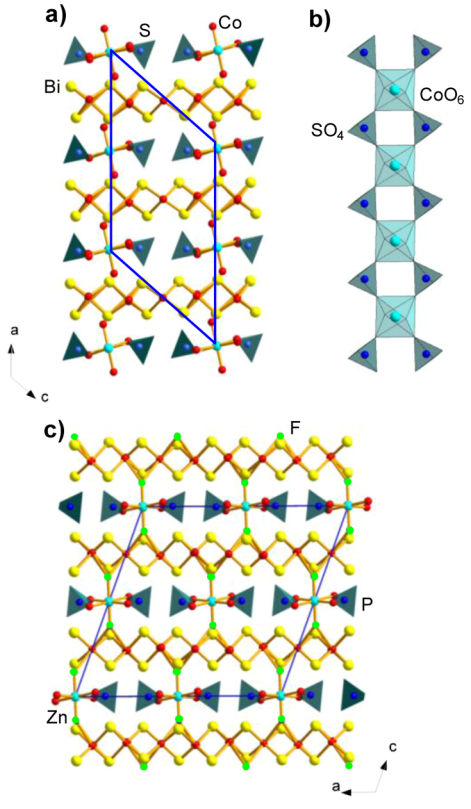

Figure 8. (a) The crystal structure of (a) $[Bi_6O_6](CoO_2)(SO_4)_2$ (compound III). (c) $[Bi_6O_6](ZnF_2)(PO_4)_2$. (b) common magnetic subunits.

shifted out of pairs of positions related by an inversion center absent in the $C2$ space group. The results of BVS are gathered in Table 3 and confirm the Co^{2+} valence and the validity of our fully ordered model with ideal bonding scheme around all cations. The crystal structure is analogous to those of reduced $Bi_4V^{5+}{}_2O_{11}$ compounds with ideal formula $[Bi_6O_6](V^{4+}O_2)(VO_4)_2$[40] and related oxo-phosphates such as $[Bi_6O_6](Ti/BiO_2)(PO_4)_2$ or $[Bi_6O_6](M/Bi,O/F_2)(PO_4)_2$ with ordering between XO_4 groups and transition metal octahedra in the interleave between $[BiO]^+$ layers.[16,17]

dx.doi.org/10.1021/ic500877z | Inorg. Chem. 2014, 53, 6969−6978

As detailed in ref 17, for these phosphates, several space groups have been reported including the *I*2 noncentrosymmetric one in the M = Ti case. Our *C*2 choice corresponds to this latter case after cell reorientation. Also it is worth mentioning that most prepared $[Bi_6O_6](M/Bi,O/F_2)(PO_4)_2$ show a statistical distribution of M^{n+} and Bi^{3+} in a common crystallographic site, while in compound the crystal structure appears fully ordered by means of our structural refinement. Finally two different stackings of the central interleave have been reported in the full series, while compound III corresponds to those called "polytype 1" in ref 17 (see Figure 8a,b). The magnetism was investigated for related compounds with various M and XO_4 groups. It shows 1D chainlike magnetism for MO_6 octahedra isolated by VO_4 groups[40] and paramagnetism for MO_6 separated by PO_4 groups.[17] In the case of sulfate, one could also expect a paramagnetic behavior according to the strongly bonded S−O bonds, unlikely for mediation of magnetic exchanges. However, as already mentioned, the amount of available amount of compound (III) obtained as single crystal in a mixture was insufficient for an accurate magnetic characterization.

CONCLUSIONS

The reinvestigation of mixed Bi/M (M = Co, Cu) oxo-sulfates leads to the revision of two previous compounds refined in the early nineties, namely, $[Bi_2CoO_3](SO_4)$ and $[Bi_{6.267}Cu_{1.6}O_8](SO_4)_3$ in which 2D layers of oxo-centerd $O(Bi,M)_4$ tetrahedra are isolated by SO_4 groups in an ordered manner. The refined models take into account supercell spots occulted in previous reports and misleading to disordered models. In those two compounds M^{2+} ions are segregated in the [(Bi,M)O] layers leading to particular topologies (Cu^{2+} dimers and Co^{2+} chains). In the Co AFM chains, measurements reveal the appearance, below ∼20 K, of canted spins with a remanent moment close to 0.2 μ_B/Co, which is probably due to Dzyaloshinski−Moriya interactions. Differently, in $[Bi_6O_6](CoO_2)(SO_4)_2$, Co ions and sulfates are ordered in the interleave, while 2D layers are made of OBi_4 only. One can suggest that the pleated character (compounds I and II) or not (compound III) of oxo-centered layers results from the sizable matching between the layers and the oxo-anion interleave. This study enlarges the panorama of inorganic compounds built up from oxo-centered tetrahedra. One shows here that this sublattice is able to hold various topologies of magnetic units, rather well-separated in terms of magnetic interactions.

ASSOCIATED CONTENT

Supporting Information

It includes detailed complementary data, such as crystallographic and computational. This material is available free of charge via the Internet at http://pubs.acs.org.

AUTHOR INFORMATION

Corresponding Author

*E-mail: olivier.mentre@ensc-lille.fr.

Notes

The authors declare no competing financial interest.

ACKNOWLEDGMENTS

The Fonds Européen de Développement Régional (FEDER), CNRS, Région Nord Pas-de-Calais, and Ministère de l'Education Nationale de l'Enseignement Supérieur et de la Recherche are acknowledged for funding the X-ray diffractometers. L. Burylo and N. Djellal are thanked for their precious technical help. This work was carried out under the framework of the Multi-InMaDe project supported by the ANR (Grant No. ANR 2011-JS-08 003 01).

REFERENCES

(1) Timmermans, C. W. M.; Blasse, G. J. *Solid State Chem.* **1984**, *52*, 222−232.
(2) Wu, S.; Wang, C.; Cui, Y.; Wang, T.; Huang, B.; Zhang, X.; Qin, X.; Brault, P. *Mater. Lett.* **2010**, *64*, 115−118.
(3) Burch, R.; Chalker, S.; Loader, P.; Thomas, J. M.; Ueda, W. *Appl. Catal., A* **1992**, *82*, 77−90.
(4) Liu, S.; Miiller, W.; Liu, Y.; Avdeev, M.; Ling, C. D. *Chem. Mater.* **2012**, *24*, 3932−C3942.
(5) Nguyen, S. D.; Yeon, J.; Kim, S.-H.; Halasyamani, P. S. *J. Am. Chem. Soc.* **2011**, *133*, 12422−12425.
(6) Fanariotis, I. A.; Rentzepeirs, P. J. *Z. Kristallogr.* **1987**, *180*, 189−194.
(7) Lagercrantz, A.; Sillen, L. G. *Ark. Kemi. Mineral Geol.* **1948**, *25a*, 1−21.
(8) Gilberg, M. *Ark. Kemi, Mineral. Geol.* **1960**, *B2*, 565.
(9) Kirik, S. D.; Yakovleva, E. G.; Shimanskii, A. F.; Kovalev, Y. G. *Acta Crystallogr., Sect. C: Cryst. Struct. Commun.* **2001**, *57*, 1367−1368.
(10) Krivovichev, S. V.; Mentré, O.; Siidra, O. I.; Colmont, M.; Filatov, S. K. *Chem. Rev.* **2013**, *113* (8), 6459−6535.
(11) Krivovichev, S. V.; Filatov, S. K. *Crystal Chemistry of Minerals and Inorganic Compounds with Complexes of Anion-Centered Tetrahedra;* St. Petersburg University Press: St. Petersburg, Russia, 2001.
(12) Huvé, M.; Colmont, M.; Lejay, J.; Aschehoug, P.; Mentré, O. *Chem. Mater.* **2009**, *21*, 4019−4029.
(13) Colmont, M.; Endara, D.; Huvé, M.; Krivovichev, S. V.; Mentré, O. *Mater. Res. Soc. Symp. Proc.* **2011**, *1309*, 15−20.
(14) Mentré, O.; Ketatni, E. M.; Colmont, M.; Huvé, M.; Abraham, F.; Petricek, V. *J. Am. Chem. Soc.* **2006**, *8*, 10857−10867.
(15) Ketatni, E. M.; Mernari, B.; Abraham, F.; Mentré, O. *J. Solid State Chem.* **2000**, *3*, 48−54.
(16) Steinfink, H.; Lynch, V. *J. Solid State Chem.* **2004**, *177*, 1412−1415.
(17) Colmont, M.; Huvé, M.; Ketatni, E. M.; Mentré, O. *Solid State Sci.* **2008**, *10*, 533−543.
(18) Lü, M. F.; Aliev, A.; Olchowka, J.; Colmont, M.; Huvé, M.; Wickleder, C.; Mentré, O. *Inorg. Chem.* **2014**, *53*, 528−536.
(19) Aurivillius, B. *Acta Chem. Scand.* **1987**, *A41*, 415.
(20) Fanariotis, I. A.; Rentzepeirs, P. J. *Z. Kristallogr.* **1991**, *194*, 261−265.
(21) Aurivillius, B. *Acta Chem. Scand.* **1991**, *45*, 769.
(22) *SAINT: Area-Detector Integration Software;* Siemens Industrial Automation, Inc.: Madison, WI, 1996.
(23) *SADABS: Area-Detector Absorption Correction;* Siemens Industrial Automation, Inc.: Madison, WI, 1995.
(24) Kresse, G.; Furthmüller, J. *Vienna Ab-initio Simulation Package (VASP);* Institut für Materialphysik: Vienna, Austria, 2004.
(25) Kresse, G.; Joubert, D. *Phys. Rev. B* **1999**, *59*, 1758.
(26) Perdew, J. P.; Wang, Y. *Phys. Rev. B* **1992**, *45*, 13244.
(27) Dudarev, S. L.; Botton, G. A.; Savrasov, S. Y.; Humphreys, C. J.; Sutton, A. P. *Phys. Rev. B* **1998**, *57*, 1505.
(28) Brown, I. D.; Altermatt, D. *Acta Crystallogr.* **1985**, *B41*, 244.
(29) David, R.; Kabbour, H.; Colis, S.; Mentre, O. *Inorg. Chem.* **2013**, *52*, 13742.
(30) Kabbour, H.; David, R.; Pautrat, A.; Koo, H.-J.; Whangbo, M.-H.; Andre, G.; Mentre, O. *Angew. Chem., Int. Ed.* **2012**, *124*, 11915−11919.
(31) Tong, J.; Kremer, R. K.; Köhler, J.; Simon, I. A.; Lee, C.; Kan, E.; Whangbo, M.-H. *Z. Kristallogr.* **2010**, *225*, 498−503.
(32) Shang, M. Y.; Chen, Y.; Tian, G.; Yuan, H. M.; Feng, S. H. *Phys. B* **2013**, *409*, 42−46.

(33) (a) Knížek, K.; Novák, P.; Jirák, Z. *Phys. Rev. B* **2005**, *71*, 054420. (b) Pardo, V.; Blaha, P.; Laskowski, R.; Baldomir, D.; Castro, J.; Schwarz, K.; Arias, J. E. *Phys. Rev. B* **2007**, *76*, 165120.
(34) Schiffer, P.; Ramirez, A. P. *Commun. Condens. Matter Phys.* **1996**, *10*, 21.
(35) Fisher, M. E. *Am. J. Phys.* **1964**, *32*, 343.
(36) Zhang, Y.; Ueda, Y. *Inorg. Chem.* **2013**, *52*, 5206−5213.
(37) Mizuno, Y.; Tohyama, T.; Makekawa, S.; Osafune, T.; Motoyama, N.; Eisaki, H.; Uchida, S. *Phys. Rev. B* **1998**, *57*, 5326.
(38) Mentre, O.; Janod, E.; Rabu, P.; Hennion, M.; Leclercq-Hugeux, F.; Kang, J.; Lee, C.; Whangbo, M.-H.; Petit, S. *Phys. Rev. B* **2009**, *80*, 180413.
(39) Crawford, H.; Richardson, H. W.; Wasson, J. R.; Hodgson, D. J.; Hatfield, W. E. *Inorg. Chem.* **1976**, *15*, 2107−2110.
(40) Joubert, O.; Jouanneaux, A.; Ganne, M. *Nucl. Instrum. Methods Phys. Res., Sect. B* **1995**, *97*, 119.